

# Pairing dome from an emergent Feshbach resonance in a strongly repulsive bilayer model

Hannah Lange,<sup>1,2,3</sup> Lukas Homeier,<sup>1,3</sup> Eugene Demler,<sup>4</sup>

Ulrich Schollwöck,<sup>1,3</sup> Annabelle Bohrdt,<sup>3,5</sup> and Fabian Grusdt<sup>1,3</sup>

<sup>1</sup>Ludwig-Maximilians-University Munich, Theresienstr. 37, Munich D-80333, Germany

<sup>2</sup>Max-Planck-Institute for Quantum Optics, Hans-Kopfermann-Str.1, Garching D-85748, Germany

<sup>3</sup>Munich Center for Quantum Science and Technology, Schellingstr. 4, Munich D-80799, Germany

<sup>4</sup>Institute for Theoretical Physics, ETH Zurich, 8093 Zürich, Switzerland

<sup>5</sup>University of Regensburg, Universitätsstr. 31, Regensburg D-93053, Germany

(Dated: November 7, 2023)

A key to understanding unconventional superconductivity lies in unraveling the pairing mechanism of mobile charge carriers in doped antiferromagnets, yielding an effective attraction between charges even in the presence of strong repulsive Coulomb interactions. Here, we study pairing in a minimal model of bilayer nickelates, featuring robust binding energies – despite dominant repulsive interactions – that are strongly enhanced in the finite doping regime. The mixed-dimensional (mixD)  $t - J$  ladder we study features a crossover from tightly bound pairs of holes (closed channel) at small repulsion, to more spatially extended, correlated pairs of individual holes (open channel) at large repulsion. We derive an effective model for the latter, in which the attraction is mediated by the closed channel, in analogy to atomic Feshbach resonances. Using density matrix renormalization group (DMRG) simulations we reveal a dome of large binding energies at around 30% doping and we observe the formation of a density wave of plaquettes consisting of two spin-charge excitation pairs on neighboring rungs. Our work paves the way towards a microscopic theory of pairing in doped quantum magnets, in particular Ni-based superconductors, and our predictions can be tested in state-of-the-art quantum simulators.

**Introduction.**—Among the remaining mysteries of high- $T_c$  superconductivity [1–3] is the pairing mechanism of charge carriers, leading to the formation of Cooper pairs [4] in a relatively high temperature regime and despite repulsive Coulomb interactions between the charges [5–7]. In contrast to conventional superconductors, for which BCS theory [8] predicts small pairing gaps that result in large Cooper pairs – effectively circumventing long-range Coulomb repulsion –, high- $T_c$  superconductors are characterized by their substantial pairing gap [9] and Cooper pairs are potentially exposed to extended-range Coulomb interactions. To investigate pairing mechanisms resilient to such Coulomb interactions, Fermi Hubbard or  $t - J$  type models have been extended to  $t - J - V$  models [10] with nearest-neighbor repulsion  $V$ . These models have been shown to sustain pairing up to large repulsion strengths [11, 12] and have proven to effectively describe some experimental results in cuprates, e.g. on plasmon spectra [13–15]. However, such models are prohibitively difficult to solve in order to unravel the underlying pairing mechanism, despite impressive numerical advances in the past years [16–19].

Ladder models have the advantage of being numerically and analytically more accessible in the full doping range. Despite their simplicity, they have been shown to feature a variety of correlated phases [20–25], including superconducting correlations even when supplementing the models with repulsive Coulomb interactions between nearest neighbors [26, 27]. Moreover, so-called mixed-dimensional (mixD) ladders, featuring hopping only along the legs but magnetic superexchange in both directions [28–30], have been shown to host bind-

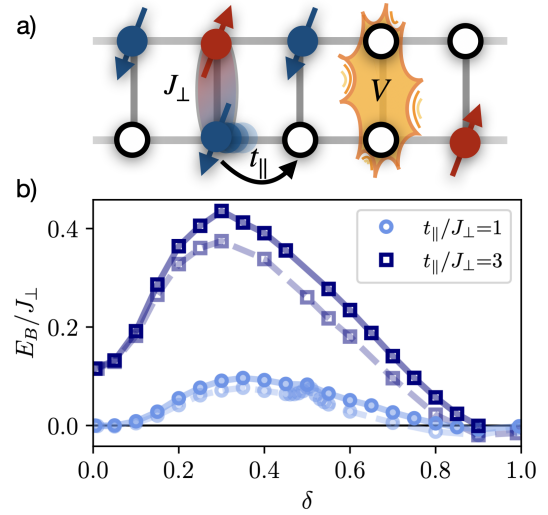


Figure 1. a) Schematic picture of the mixD ladder, with exchange coupling  $J_{\perp}$  between the legs and hopping  $t_{\parallel}$  only along the legs. Furthermore, we consider a repulsive interaction  $V$  between holes on the same rung. b) Binding energies for different values of the hole doping  $\delta = \frac{N_h}{L_x \cdot L_y}$ , for  $\frac{V}{J_{\perp}} = 5$  and  $L_x = 100$  (dashed lines) and  $L_x = 200$  (solid lines).

ing on extremely high energy scales, even exceeding the superexchange energy [30, 31]. This allows to observe binding [30, 31] and stripe formation [32] in these models using ultracold atom experiments [29, 33–36], where experimentally reachable temperatures are today typically on the order of the superexchange energy [34]. Furthermore, recent works proposed that the high-temperature superconductor  $\text{La}_3\text{Ni}_2\text{O}_7$  can be modeled by mixD bilayers, see e.g. Refs. [37–42].

Here, we utilize mixD models as a controlled setting to study the rich interplay of magnetic fluctuations, Coulomb repulsion and arbitrary doping, see Fig. 1. Such mixD models host interesting emergent structures: When the half-filled ground state of a ladder with small intra-leg superexchange  $0 \leq J_{\parallel} \ll J_{\perp}$  is doped with a single hole, the latter can be understood as a bound state of two partons, a *chargon* and *spinon*, carrying the respective quantum numbers and being connected by a linear confinement potential [29, 30], as observed also in 2D [43–50]. Similarly, two holes form a pair of two chargons in the mixD setting [30, 31]. In analogy to mesons in high energy physics, the constituents (*partons*) of this pair are very tightly bound, and hence the chargon-chargeon bound state will also be referred to as *meson* in the following. In this letter we show that strong interactions – approximating the Coulomb repulsion of electrons in solids – favor another pairing scenario which, we argue, is more closely related to the pairing seen in most real materials: more extended Cooper-type bound states of two mesons, i.e. consisting of four constituents (*tetrapartons*).

Specifically, we investigate a mixD  $t - J$  ladder supplemented with strong repulsive interactions  $V$  between two holes on a rung (see Fig. 1a) – i.e. an off-site repulsion that may also be relevant in nickelate superconductors. Combining DMRG simulations [51, 52] and effective descriptions in terms of the emergent charge carriers we show that the effective attraction between the holes in the large  $V$  regime is induced by coupling processes to the chargon-chargeon, meson-like states. To highlight the analogy of this mechanism to Feshbach resonances [53], we refer to the high energy channel of chargon-chargeon (cc) states as closed, mesonic channel and to the low energy spinon-chargeon (sc) pairs as the open, tetraparton channel at large  $V$ .

Overall, the mixD ladders we study show some remarkable phenomenological similarities with strongly correlated superconductors such as cuprates and nickelates: (i) We report pairing facilitated by doping, leading to a dome of binding energies with its peak at 30% doping (see Fig 1b); (ii) the pairing we find only requires short-range antiferromagnetic (AFM) correlations but no long-range magnetic order; (iii) we discover a density wave (with bond order) in the intermediate doping regime.

**Model and emergent constituents.**–The primary goal of this work is to investigate the impact of strong repulsive interactions  $V$  on the pairing mechanism in a mixD ladder, featuring inter-leg exchange interactions but no inter-leg tunneling [28, 30, 31], see Fig. 1a,

$$\hat{\mathcal{H}} = -t_{\parallel} \hat{\mathcal{P}} \sum_j \sum_{\mu, \sigma} \left( \hat{c}_{j+1\mu\sigma}^{\dagger} \hat{c}_{j\mu\sigma} + \text{h.c.} \right) \hat{\mathcal{P}} + J_{\perp} \sum_j \left( \hat{\mathbf{S}}_{j0} \cdot \hat{\mathbf{S}}_{j1} - \frac{1}{4} \hat{n}_{j0} \hat{n}_{j1} \right) + V \sum_j \hat{n}_{j0}^h \hat{n}_{j1}^h. \quad (1)$$

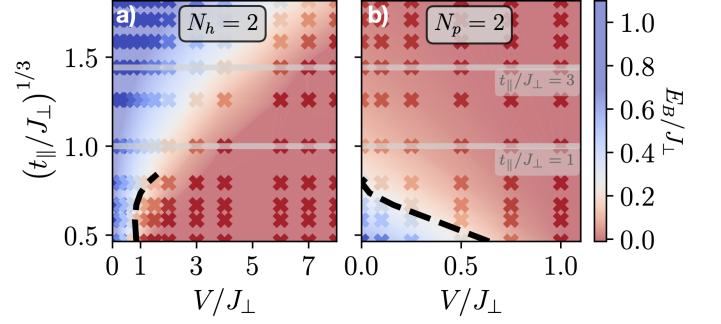


Figure 2. Binding energy in the limits of a) low ( $N_h = 2$ ) and b) high ( $N_p = L_x \cdot L_y - N_h = 2$ ) doping. If  $t_{\parallel} \ll V, J_{\perp}$  the critical  $V_c$  values for which cc’s do not constitute the ground state any more are denoted by the black dotted lines (see [55]). Here, we expect the crossover to the sc regime.

Here,  $\hat{\mathcal{P}}$  is the Gutzwiller projector onto the subspace with maximum single occupancy per site. Spin operators at site  $j \in \{1, \dots, L_x\}$  in leg  $\mu = 0, 1$  are denoted by  $\hat{\mathbf{S}}_{j\mu}$ , (hole) density operators by  $\hat{n}_{j\mu} = \hat{n}_{j\mu\uparrow} + \hat{n}_{j\mu\downarrow}$  ( $\hat{n}_{j\mu}^h = 1 - \hat{n}_{j\mu}$ ), and  $\hat{c}_{j\mu\sigma}$  annihilate a fermion with spin  $\sigma = \uparrow, \downarrow$ .

At half-filling, the ground state of the system is given by spin singlets on each rung [30]. At finite doping the system is dominated by a competition of the kinetic energy and the energy of the distortion of the spin background when holes move. The emergent constituents in this doping regime are most easily understood when  $t_{\parallel} \ll J_{\perp}$ . At  $V = 0 \leq t_{\parallel} \ll J_{\perp}$  two holes tend to sit on the same rung – a configuration with energy  $-J_{\perp}$  – and form a chargon-chargeon pair (cc), see Fig. 3a left. They can move freely through the system, since the second chargon restores the spin-singlet background when following the first one, making it favorable for charges to move through the system together, i.e. yielding large binding energies [30]. When the repulsive interaction  $V$  reaches a critical value  $V_c$ , it is energetically favorable to place at maximum one hole (and one spin) per rung, i.e. to form a spinon-chargeon pair (sc), see Fig. 3a right. In contrast to cc’s, the motion of sc’s is suppressed by the distortion of the singlet spin-background created when the chargon moves.

When  $t_{\parallel} > J_{\perp}$ , this meson picture remains qualitatively correct, although the cc’s and sc’s develop a finite spatial extent determined by the interplay of the kinetic energy and a linear confining potential (a *string*) between the partons [30, 49]; see also [54]. As we show in the following sections, the crossover from the cc ( $V < V_c$ ) to the sc regime ( $V > V_c$ ) depends strongly on the ratio  $t_{\parallel}/J_{\perp}$ , i.e.  $V_c = V_c(t_{\parallel}/J_{\perp})$ .

**Limits of low and high doping.**– Using the DMRG package SyTen [56, 57] with  $U(1)_{N_{\mu=1,2}}$  symmetry on each leg and global  $U(1)_{S_z^{\text{tot}}}$  symmetry, we calculate the binding energies defined by

$$E_B(N_h) = 2(E_{N_h-1} - E_{N_h-2}) - (E_{N_h} - E_{N_h-2}), \quad (2)$$

where  $N_h$  is the number of holes doped in the system

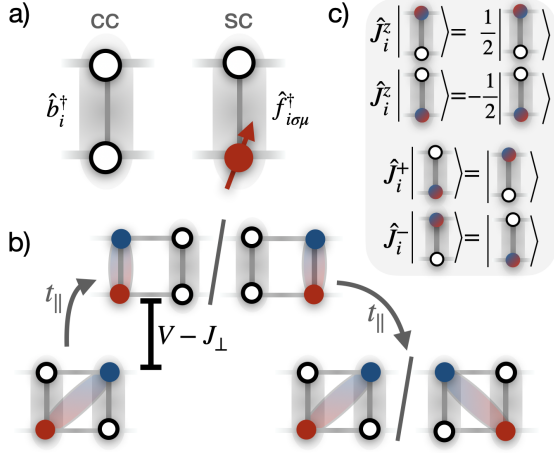


Figure 3. a) The constituents of the effective theory in the large  $V$  limit: chargin-chargin (cc) and spinon-chargin (sc) pairs, denoted by  $\hat{b}_i^{(\dagger)}$  and  $\hat{f}_{i\sigma\mu}^{(\dagger)}$  respectively, for  $i \in \{1 \dots L_x\}$ . b) Schrieffer-Wolff transformation for  $V, V - J_\perp \gg t_\parallel$  with the low-energy sc and high energy cc subspaces. c) Definition of the leg isospin operator  $\hat{J}_i$  as introduced formally in Eq. (4).

and  $E_B > 0$  indicates binding of holes. Details on the implementation can be found in [54].

Our results in the limits of very low ( $N_h = 2$ ) and high ( $N_p = L_x \cdot L_y - N_h = 2$ ) doping are shown in Fig. 2. For  $t_\parallel = 0$  the cc at low doping and the particle pair at high doping are bound by the fact that it is energetically favorable to form singlets on the rungs. In both cases, the pairs unbind when  $V \geq V_c(t_\parallel = 0) = J_\perp$ .

For  $t_\parallel \ll J_\perp$  we perform a Schrieffer-Wolff transformation, as detailed further below, to estimate the critical value  $V_c$ , where the nature of the constituents changes from tightly bound cc's to weakly bound sc's in the low and high hole doping regimes [29], see [55]. The resulting perturbative expressions for  $V_c$ , indicated by the dashed black lines in Fig. 2, agree well with the numerical results for  $t_\parallel \leq J_\perp$ . At low doping, Fig. 2a, even the backbending observed numerically is captured correctly. Furthermore, analytics and numerics show that the low and high doping regimes are distinctly different: (a) For two holes, the string-based pairing mechanism [30] yields pronounced binding even for large  $t_\parallel/J_\perp$ . For example, for  $t_\parallel/J_\perp = 3$ , a repulsion  $V > 7J_\perp$  is needed to suppress the binding energy below  $E_B/J_\perp = 10\%$ , coinciding with the numerical observation of widely spread hole pairs over more than 20 sites for a system of length  $L_x = 80$  (see [54]). (b) In the high doping limit with only two particles remaining in the system, the binding energy is suppressed to very small values  $E_B/J_\perp < 0.01$  as soon as  $V \approx J_\perp$ . For large  $t_\parallel \geq J_\perp$ , the perturbative description breaks down.

**Strong pairing at finite doping.**—For large  $V$ , we show in Fig. 2 that neither very low nor very high doping permits significant pairing of charges. Remarkably, we find drastically enhanced binding energies at interme-

diated doping values in Fig. 1b, where  $V = 5J_\perp$ : For both hopping strengths,  $E_B$  shows a pronounced dome around  $\delta_{\text{opt}} \approx 30\%$  doping, before decreasing again down to a vanishingly small value for the two-particle system. At  $t_\parallel/J_\perp = 3$ , where the pairing is already strong at low doping, the binding energies increase by around a factor of 3 at  $\delta \approx 30\%$  doping. For  $t_\parallel/J_\perp = 1$ , where binding is strongly suppressed at  $N_h = 2$ , doping leads to an increase of the binding energies by a factor  $> 10$ .

To gain a better understanding of the binding energies in the finite doping regime we derive an effective model for  $V > t_\parallel, J_\perp$  – a regime for which sc configurations are dominant. In this limit of large  $V > J_\perp \gg t_\parallel$  we identify two subspaces of (i) sc constituents at low energy and (ii) cc configurations that are gapped by  $\Delta E = V - J_\perp$ . We perform a Schrieffer-Wolff transformation [58] of Eq. (1) assuming small  $|t_\parallel/\Delta E|$  and integrate out the cc states, see Fig. 3b. We express the effective Hamiltonian in terms of sc operators  $\hat{f}_{i\mu\sigma}^{(\dagger)}$  which act on the vacuum state consisting of rung-singlets. At  $V > J_\perp \gg t_\parallel$  at maximum one sc is allowed per rung, which we enforce by the projector  $\hat{\mathcal{P}}_f$  on the corresponding subspace. Moreover, the effective Hamiltonian only applies below  $\delta \leq 50\%$  doping, before cc's naturally proliferate. We find (see [54] for derivation):

$$\begin{aligned} \hat{\mathcal{H}}_{\text{eff}}^{\text{sc}} = & \frac{t_\parallel}{2} \sum_j \sum_{\sigma, \mu} \hat{\mathcal{P}}_f \left( \hat{f}_{j+1\mu\sigma}^\dagger \hat{f}_{j\mu\sigma} + \text{h.c.} \right) \hat{\mathcal{P}}_f \\ & + \epsilon_0 \sum_{j\mu} \hat{n}_{i\mu}^f + \frac{t_\parallel^2}{J_\perp} \frac{3}{2} \sum_j \sum_{\mu\mu'} \hat{n}_{j+1\mu}^f \hat{n}_{j\mu'}^f \\ & - 4t_\parallel^2 \sum_j \left( -\hat{\mathbf{J}}_{j+1} \cdot \hat{\mathbf{J}}_j + \frac{1}{4} \right) \left[ \frac{\hat{\mathcal{P}}_j^S}{V - J_\perp} + \frac{\hat{\mathcal{P}}_j^T}{V} \right]. \quad (3) \end{aligned}$$

Here, we have defined  $\epsilon_0 = J_\perp - \frac{t_\parallel^2}{J_\perp} \frac{3}{2}$  and the singlet and triplet projectors  $\hat{\mathcal{P}}_j^S = -\hat{\mathbf{S}}_{j+1} \cdot \hat{\mathbf{S}}_j + \frac{1}{4} \hat{n}_{j+1}^f \hat{n}_j^f$  and  $\hat{\mathcal{P}}_j^T = \hat{\mathbf{S}}_{j+1} \cdot \hat{\mathbf{S}}_j + \frac{3}{4} \hat{n}_{j+1}^f \hat{n}_j^f$ , with the sc density operators  $\hat{n}_{j\mu}^f = \sum_\sigma \hat{f}_{j\mu\sigma}^\dagger \hat{f}_{j\mu\sigma}$ , the sc spin operators  $\hat{\mathbf{S}}_j = \frac{1}{2} \sum_\mu \sum_{\sigma\sigma'} \hat{f}_{j\mu\sigma}^\dagger \boldsymbol{\sigma}_{\sigma\sigma'} \hat{f}_{j\mu\sigma'}$  and isospin leg operators (see Fig. 3c)

$$\hat{\mathbf{J}}_j = \frac{1}{2} \sum_\sigma \sum_{\mu\mu'} \hat{f}_{j\mu\sigma}^\dagger \boldsymbol{\sigma}_{\mu\mu'} \hat{f}_{j\mu'\sigma}. \quad (4)$$

Eq. (3) describes hard-core, fermionic sc's, experiencing repulsive (3rd term) and attractive interactions  $\propto \frac{t_\parallel^2}{V - J_\perp}$  and  $\propto \frac{t_\parallel^2}{V}$  (4th term with negative sign for spin singlet / triplet configurations and leg singlets) that compete with each other. We emphasize that the attraction is mediated by virtual processes involving the high-energy cc channel shown in Fig. 3b, similar to the attraction induced at a Feshbach resonance. This is also apparent from the term  $\propto \hat{\mathbf{J}}_{j+1} \cdot \hat{\mathbf{J}}_j$  which penalizes neighboring

sc's occupying the same leg, since only sc's from opposite legs can lower their energy by recombining virtually into the cc channel. Furthermore, a resonance occurs at  $V \rightarrow J_\perp$ , where the attractive interaction diverges and becomes dominant over the repulsion.

The Feshbach-mediated pairing mechanism in Eq. (3) is in qualitative agreement with the doping dependence of the binding energies in Fig. 1b. Near the resonance, when the attraction is dominant, the attractive interactions predicted by Eq. (3) are effectively enhanced when the number of holes in the system is increased, since the kinetic energy per hole decreases with doping (Pauli pressure). This suggests an increasing binding energy with doping, i.e. when the number of sc's increases, similar to the dome of  $E_B$  in Fig. 1b. The optimal doping  $\delta_{\text{opt}}$ , corresponding to maximum binding energy, is reached when sc's begin to overlap spatially: In the effective model (3) of point-like sc's, this suggests a maximum at  $\delta_{\text{opt}} = 50\%$ , in agreement with our numerical results on the full mixD system as well as on the effective sc model for  $t_\parallel \ll J_\perp$  [54]. For larger  $t_\parallel \geq J_\perp$ , we expect that the mechanism remains essentially the same, but with two main changes: (i) Since binding is stabilized by  $t_\parallel$ , the resonance shifts to higher values  $V_c > J_\perp$ , yielding positive binding energies even for large  $V = 5J_\perp$  at finite doping that are on the same order of magnitude as in Fig. 1, see Ref. [54]. (ii) sc's extend over several rungs and  $\delta_{\text{opt}}$  shifts to smaller values  $< 50\%$ , as in Fig. 1b.

Another remarkable feature of the effective model (3) is the emergent isospin  $SU(2)$  symmetry. We find numerical indications that this  $SU(2)$  symmetry is only approximately present in the full mixD system (1), see [55], with a strong doping dependence, see also Ref. [54]. When higher orders in  $t_\parallel/\Delta E$  are considered, the  $SU(2)$  isospin symmetry of Eq. (3) breaks down.

**Bond order at 50% doping.**—In the large  $V$  limit, no more than one sc can occupy each rung. This leads to a charge gap at commensurate filling  $\delta = 50\%$ , corresponding to the energy required to create a cc. From our analytical model we hence conclude that the existence of such a charge gap provides a direct signature for the signature of the underlying constituents in the finite-doping regime.

The remaining spin ( $\hat{S}_j$ ) and leg (isospin  $\hat{J}_j$ ) degrees of freedom at  $\delta = 50\%$  are described by the effective Hamiltonian

$$\hat{\mathcal{H}}_{\text{eff}}^{sc, \delta=1/2} = 4 \frac{t_\parallel^2}{V} \sum_j \left( \hat{J}_{j+1} \cdot \hat{J}_j - \frac{1}{4} \right) \cdot \left[ 1 + \frac{J_\perp}{V} \hat{P}_j^S \right] \quad (5)$$

obtained directly from Eq. (3) when  $V \gg J_\perp, t_\parallel$  (see [54]).

At  $J_\perp = 0$ , the ground state of Eq. (5) is a 1D Heisenberg AFM of the isospin  $\hat{J}$ , with power-law correlations, and is fully degenerate in the spin  $\hat{S}$ . In contrast, for large  $J_\perp/V$  we expect the ground state to be a correlated

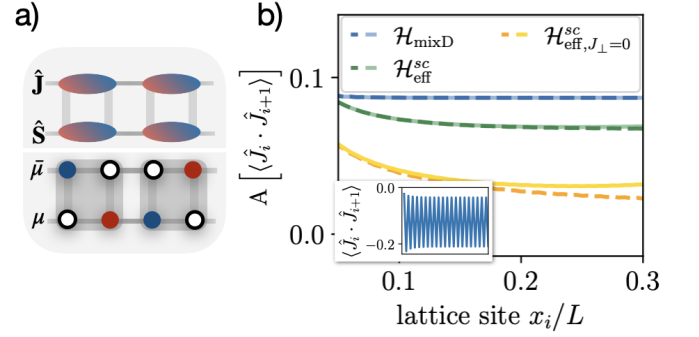


Figure 4. a) Illustration of the bond-ordered phase for  $\delta = 0.5$  and  $V, V - J_\perp \gg t_\parallel$ : the system forms plaquettes of  $\hat{S}$  and  $\hat{J}$ -singlets. b) This yields strong oscillations of  $\langle \hat{J}_i \cdot \hat{J}_{i+1} \rangle$  and  $\langle \hat{S}_i \cdot \hat{S}_{i+1} \rangle$  throughout the system with amplitudes  $A [\langle \hat{J}_i \cdot \hat{J}_{i+1} \rangle]$  for  $V/J_\perp = 5, t_\parallel/J_\perp = 1$  (blue lines). We compare our results to predictions by the effective model Eq. (5) for  $J_\perp = 1$  (green) and for  $J_\perp = 0$  (orange) with  $L_x = 100$  (light solid lines) and  $L_x = 200$  (dashed).

valence-bond crystal (VBS) of both spin and isospins, i.e. an alternating pattern of singlets (no singlets) on bonds  $\langle 2j, 2j+1 \rangle$  ( $\langle 2j+1, 2j+2 \rangle$ ) as illustrated in Fig. 4a. This state has a lower variational energy contribution for the second term in Eq. (5) per bond than two independent AFM Heisenberg chains for  $\hat{J}$  and  $\hat{S}$  (see [54]); it corresponds to a bond-ordered phase of interacting spinon-chargeon Cooper pairs (*bond-ordered density wave*, *BODW*) on plaquettes.

Our analytical prediction of correlated VBS order in  $\hat{J}$  and  $\hat{S}$  is supported even for moderate values of  $V/J_\perp = 5$  by our numerical results for the mixD model, Eq. (1); blue in Fig. 4b. These show that oscillating expectation values  $\langle \hat{J}_i \cdot \hat{J}_{i+1} \rangle$  and  $\langle \hat{S}_i \cdot \hat{S}_{i+1} \rangle$  (see inset in Fig. 4b), corresponding to the singlet (minima) and no-singlet (maxima) BODW order.

While the pure 1D spin- $\frac{1}{2}$  Heisenberg model shows similar VBS-like oscillations in finite-size systems with open boundaries, their amplitude decays notably when increasing the system size. We confirm this behavior for  $\langle \hat{J}_i \cdot \hat{J}_{i+1} \rangle$  at  $J_\perp = 0$  in Fig. 4b (orange), and contrast it with the robust VBS correlations, essentially without any remaining finite size dependence, which we find for  $V/J_\perp = 5$  at  $t_\parallel = J_\perp$ , see Fig. 4b, both for the mixD model (1) (blue) and the effective sc model (3) (green).

**Experimental Realizations.**—Our studies are motivated by recent experiments in cold atoms and nickelate compounds:

The mixD model without repulsion  $V$  was already realized in a setup of ultracold fermionic atoms in an optical potential [31] by applying a potential offset  $\Delta$  between the legs to suppress the inter-leg tunneling  $\hat{t}_\perp$  to an effective  $t_\perp \approx 0$ . To supplement this setup with a nearest-neighbors repulsion, we propose hole (doublon) doping

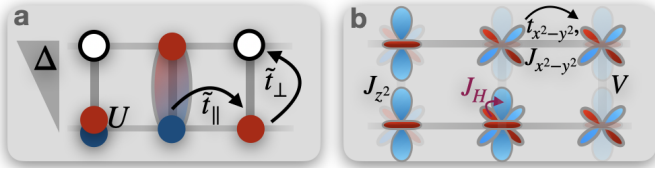


Figure 5. a) The ultracold atom setup for a mixD ladder with repulsion: a potential offset  $\Delta$  and hole (doublon) doping in the upper (lower) leg are shown. b) Schematic illustration of the bilayer  $\text{La}_3\text{Ni}_2\text{O}_7$ :  $d_{x^2-y^2}$  orbitals contribute to intralayer hopping and AFM exchange,  $d_z^2$  orbitals to an interlayer AFM exchange and both orbitals are coupled by FM Hund's coupling  $J_H$ .

for upper (lower) legs of the ladder, see Fig. 5a. This gives rise to virtual hopping processes between doublons in the lower leg and holes in the upper leg with amplitude  $2\frac{\tilde{t}_\perp^2}{\Delta}$  and doublons and spins with  $\frac{\tilde{t}_\perp^2}{\Delta+U}$ , yielding a total interaction strength  $V = 2\tilde{t}_\perp^2 \frac{U}{\Delta(U-\Delta)}$  [54].

Furthermore, as recently discussed in Ref. [39], the recently discovered nickelate superconductor  $\text{La}_3\text{Ni}_2\text{O}_7$  [37] can be modeled by a bilayer  $t_\parallel - J_\parallel - J_\perp$  similar to the model we study. In this material, the  $d_{x^2-y^2}$  orbitals form an effective intralayer  $t_{x^2-y^2} - J_{x^2-y^2}$  model, whereas the  $d_z^2$  orbitals are localized with interlayer antiferromagnetic (AFM) superexchange, see Fig. 5b. Both orbitals interact via ferromagnetic (FM) Hund's coupling  $J_H$ . In the limit of large  $J_H$  the spins of  $d_{x^2-y^2}$  and  $d_z^2$  form triplets, giving rise to an effective AFM interaction  $J_\perp$  of  $d_{x^2-y^2}$  spins between the layers [39, 40]. In contrast to AFM interactions solely originating from superexchange, the interaction mediated via Hund's rule yields vanishingly small interlayer hopping. We argue that in such a 2D material the Coulomb repulsion  $V$  may play an important role at low doping. The effective sc model (3) is also valid for this 2D bilayer system.

**Summary and Outlook.**—Our results show that effective attractive interactions between charge carriers can arise even in the presence of strong repulsive interactions, here in the setting of a mixD  $t-J$  ladder. The binding energies we observe feature a pronounced maximum in the intermediate doping regime. We demonstrate that the system in this strong repulsion regime can be understood in terms of correlated sc's ((sc)<sup>2</sup>). This picture implies the formation of a BODW at a hole doping of 50% that is also observed in our numerics, with plaquettes consisting of two spinon-chargon pairs, i.e. four constituents: these form singlets in terms of spin and leg indices.

While the BODW is gapped in charge and spin sectors, the state that we observe away from 50% hole doping is a Luther-Emery liquid of (sc)<sup>2</sup> pairs with no charge gap but a spin gap, as we analyze in more detail in Ref. [54]. Similar to works on atomic BEC-BCS crossovers (e.g. [59–62]), where binding in the Luther-Emery state is induced by a narrow Feshbach resonance with a closed

channel of bosonic molecules [62], our mixD model results suggest that binding in the (sc)<sup>2</sup> regime arises from coupling to the closed cc channel. For a more detailed analysis of the Feshbach resonance and the change of the emergent charge carriers' nature, spectroscopic measurements in both regimes could be envisioned.

Finally, our results may have implications for understanding pairing in high- $T_c$  cuprate compounds [63] and recently discovered bilayer Ni-based superconductors [37]. In the context of the latter, our model can be seen as an extension of previously studied mixD  $t_\parallel - J_\parallel - J_\perp$  models [38–42] to finite-range Coulomb repulsion that should also be present in these materials. Extending our analysis to mixD bilayers [30] at finite doping will be an important step towards a microscopic description of the underlying pairing mechanism in these materials.

*Note added.*— After submission of our manuscript to the pre-print server, we became aware of a closely related work by H. Yang, H. Oh and Y. H. Zhang [64], in which they use the DMRG method to study a similar bilayer repulsive  $t-J$  model on a two-leg ladder. In their work, they also find the emergence of Feshbach resonance and propose a doping induced BEC-to-BCS crossover scenario for the bilayer nickelates.

*Acknowledgements.*— We would like to thank Atac Imamoglu, Daniel Jirovec, Felix Palm, Henning Schlömer, Immanuel Bloch, Ivan Morera Navarro, Lieven Vandersypen, Markus Greiner, Matjaz Kebric, Pablo Cova Farina, Tim Harris and Tizian Blatz for helpful discussions. Special thanks to Henning Schlömer for his help with the DMRG implementation of the mixD symmetries. We acknowledge funding by the Deutsche Forschungsgemeinschaft (DFG, German Research Foundation) under Germany's Excellence Strategy – EXC-2111 – 390814868 and from the European Research Council (ERC) under the European Union's Horizon 2020 research and innovation program (Grant Agreement no 948141) — ERC Starting Grant SimUcQuam. ED acknowledges support from the ARO grant W911NF-20-1-0163 and the SNSF project 200021-212899. HL acknowledges support by the International Max Planck Research School. LH acknowledges support by Studienstiftung des deutschen Volkes.

- [1] J. G. Bednorz and K. A. Müller, *Zeitschrift für Physik B Condensed Matter* **64**, 189 (1986).
- [2] P. A. Lee, N. Nagaosa, and X.-G. Wen, *Rev. Mod. Phys.* **78**, 17 (2006).
- [3] D. J. Scalapino, *Journal of Low Temperature Physics* **117**, 179 (1999).
- [4] L. N. Cooper, *Phys. Rev.* **104**, 1189 (1956).
- [5] W. Kohn and J. M. Luttinger, *Phys. Rev. Lett.* **15**, 524 (1965).

- [6] A. Kantian, M. Dolfi, M. Troyer, and T. Giamarchi, *Phys. Rev. B* **100**, 075138 (2019).
- [7] S. Chakravarty and S. A. Kivelson, *Phys. Rev. B* **64**, 064511 (2001).
- [8] J. Bardeen, *Phys. Rev.* **97**, 1724 (1955).
- [9] M. Hashimoto, I. M. Vishik, R.-H. He, T. P. Devereaux, and Z.-X. Shen, *Nature Physics* **10**, 483 (2014).
- [10] L. F. Feiner, J. H. Jefferson, and R. Raimondi, *Phys. Rev. B* **53**, 8751 (1996).
- [11] Q.-H. Wang, J. H. Han, and D.-H. Lee, *Phys. Rev. B* **65**, 054501 (2001).
- [12] L. Zinni, M. Bejas, and A. Greco, *Phys. Rev. B* **103**, 134504 (2021).
- [13] M. Hepting, T. D. Boyko, V. Zimmermann, M. Bejas, Y. E. Suyolcu, P. Puphal, R. J. Green, L. Zinni, J. Kim, D. Casa, M. H. Upton, D. Wong, C. Schulz, M. Bartkowiak, K. Habicht, E. Pomjakushina, G. Cristiani, G. Logvenov, M. Minola, H. Yamase, A. Greco, and B. Keimer, *Phys. Rev. B* **107**, 214516 (2023).
- [14] A. Greco, H. Yamase, and M. Bejas, *Phys. Rev. B* **94**, 075139 (2016).
- [15] A. Greco, H. Yamase, and M. Bejas, *Communications Physics* **2**, 3 (2019).
- [16] M. Qin, C.-M. Chung, H. Shi, E. Vitali, C. Hubig, U. Schollwöck, S. R. White, and S. Zhang (Simons Collaboration on the Many-Electron Problem), *Phys. Rev. X* **10**, 031016 (2020).
- [17] T. Schäfer, N. Wentzell, F. Šimkovic, Y.-Y. He, C. Hille, M. Klett, C. J. Eckhardt, B. Arzhang, V. Harkov, F. m. c.-M. Le Régent, A. Kirsch, Y. Wang, A. J. Kim, E. Kozik, E. A. Stepanov, A. Kauch, S. Andergassen, P. Hansmann, D. Rohe, Y. M. Vilk, J. P. F. LeBlanc, S. Zhang, A.-M. S. Tremblay, M. Ferrero, O. Parcollet, and A. Georges, *Phys. Rev. X* **11**, 011058 (2021).
- [18] H. Xu, C.-M. Chung, M. Qin, U. Schollwöck, S. R. White, and S. Zhang, “Coexistence of superconductivity with partially filled stripes in the hubbard model,” (2023), [arXiv:2303.08376](https://arxiv.org/abs/2303.08376) [cond-mat.supr-con].
- [19] D. P. Arovas, E. Berg, S. A. Kivelson, and S. Raghu, *Annual Review of Condensed Matter Physics* **13**, 239 (2022), <https://doi.org/10.1146/annurev-conmatphys-031620-102024>.
- [20] E. Dagotto, J. Riera, and D. Scalapino, *Phys. Rev. B* **45**, 5744 (1992).
- [21] M. Sigrist, T. M. Rice, and F. C. Zhang, *Phys. Rev. B* **49**, 12058 (1994).
- [22] Z. Zhu, H.-C. Jiang, D. N. Sheng, and Z.-Y. Weng, *Scientific Reports* **4**, 5419 (2014).
- [23] Y.-H. Zhang and A. Vishwanath, *Phys. Rev. B* **106**, 045103 (2022).
- [24] H.-K. Zhang, R.-Y. Sun, and Z.-Y. Weng, “Pair density wave characterized by a hidden string order parameter,” (2022), [arXiv:2212.06170](https://arxiv.org/abs/2212.06170) [cond-mat.str-el].
- [25] H.-C. Jiang, S. Chen, and Z.-Y. Weng, *Phys. Rev. B* **102**, 104512 (2020).
- [26] E. Dagotto and J. Riera, *Phys. Rev. B* **46**, 12084 (1992).
- [27] M. Troyer, *Simulation of constrained fermions in low-dimensional systems*, Ph.D. thesis, ETH Zurich, <https://doi.org/10.3929/ethz-a-001371728> (1994).
- [28] F. Grusdt, Z. Zhu, T. Shi, and E. Demler, *SciPost Physics* (2018).
- [29] A. Bohrdt, L. Homeier, C. Reinmoser, E. Demler, and F. Grusdt, *Annals of Physics* **435**, 168651 (2021), special issue on Philip W. Anderson.
- [30] A. Bohrdt, L. Homeier, I. Bloch, E. Demler, and F. Grusdt, *Nature Physics* **18**, 651 (2022).
- [31] S. Hirthe, T. Chalopin, D. Bourgund, P. Bojović, A. Bohrdt, E. Demler, F. Grusdt, I. Bloch, and T. A. Hilker, *Nature* **613**, 463 (2023).
- [32] H. Schlömer, A. Bohrdt, L. Pollet, U. Schollwöck, and F. Grusdt, “Robust stripes in the mixed-dimensional  $t-j$  model,” (2022).
- [33] R. A. Hart, P. M. Duarte, T.-L. Yang, X. Liu, T. Paiva, E. Khatami, R. T. Scalettar, N. Trivedi, D. A. Huse, and R. G. Hulet, *Nature* **519**, 211 (2015).
- [34] A. Mazurenko, C. S. Chiu, G. Ji, M. F. Parsons, M. Kánász-Nagy, R. Schmidt, F. Grusdt, E. Demler, D. Greif, and M. Greiner, *Nature* **545**, 462 (2017).
- [35] I. Bloch, J. Dalibard, and W. Zwerger, **80**, 885 (2008).
- [36] C. Gross and I. Bloch, *Science* **357**, 995 (2017), <https://www.science.org/doi/pdf/10.1126/science.aal3837>.
- [37] H. Sun, M. Huo, X. Hu, J. Li, Z. Liu, Y. Han, L. Tang, Z. Mao, P. Yang, B. Wang, J. Cheng, D.-X. Yao, G.-M. Zhang, and M. Wang, *Nature* (2023), 10.1038/s41586-023-06408-7.
- [38] W. Wú, Z. Luo, D.-X. Yao, and M. Wang, “Charge transfer and zhang-rice singlet bands in the nickelate superconductor  $\text{La}_3\text{Ni}_2\text{O}_7$  under pressure,” (2023), [arXiv:2307.05662](https://arxiv.org/abs/2307.05662) [cond-mat.str-el].
- [39] C. Lu, Z. Pan, F. Yang, and C. Wu, “Interlayer coupling driven high-temperature superconductivity in  $\text{la}_3\text{ni}_2\text{o}_7$  under pressure,” (2023), [arXiv:2307.14965](https://arxiv.org/abs/2307.14965) [cond-mat.supr-con].
- [40] X.-Z. Qu, D.-W. Qu, J. Chen, C. Wu, F. Yang, W. Li, and G. Su, “Bilayer  $t-j-j_\perp$  model and magnetically mediated pairing in the pressurized nickelate  $\text{la}_3\text{ni}_2\text{o}_7$ ,” (2023), [arXiv:2307.16873](https://arxiv.org/abs/2307.16873) [cond-mat.str-el].
- [41] Z. Luo, X. Hu, M. Wang, W. Wú, and D.-X. Yao, “Bilayer two-orbital model of  $\text{la}_3\text{ni}_2\text{o}_7$  under pressure,” (2023), [arXiv:2305.15564](https://arxiv.org/abs/2305.15564) [cond-mat.supr-con].
- [42] Y. Gu, C. Le, Z. Yang, X. Wu, and J. Hu, “Effective model and pairing tendency in bilayer ni-based superconductor  $\text{la}_3\text{ni}_2\text{o}_7$ ,” (2023), [arXiv:2306.07275](https://arxiv.org/abs/2306.07275) [cond-mat.supr-con].
- [43] W. F. Brinkman and T. M. Rice, *Phys. Rev. B* **2**, 1324 (1970).
- [44] S. A. Trugman, *Phys. Rev. B* **37**, 1597 (1988).
- [45] P. Béran, D. Poilblanc, and R. B. Laughlin, *Nuclear Physics B* **473**, 707 (1996).
- [46] R. B. Laughlin, *Phys. Rev. Lett.* **79**, 1726 (1997).
- [47] T. Senthil, S. Sachdev, and M. Vojta, *Phys. Rev. Lett.* **90**, 216403 (2003).
- [48] F. Grusdt, M. Kánász-Nagy, A. Bohrdt, C. S. Chiu, G. Ji, M. Greiner, D. Greif, and E. Demler, *Phys. Rev. X* **8**, 011046 (2018).
- [49] F. Grusdt, A. Bohrdt, and E. Demler, *Physical Review B* **99**, 224422 (2019).
- [50] C. S. Chiu, G. Ji, A. Bohrdt, M. Xu, M. Knap, E. Demler, F. Grusdt, M. Greiner, and D. Greif, *Science* **365**, 251 (2019), <https://www.science.org/doi/pdf/10.1126/science.aav3587>.
- [51] S. R. White, *Phys. Rev. Lett.* **69**, 2863 (1992).
- [52] U. Schollwöck, *Annals of Physics* **326**, 96 (2011).
- [53] H. Feshbach, *Annals of Physics* **5**, 357 (1958).
- [54] H. Lange, L. Homeier, E. Demler, U. Schollwöck, F. Grusdt, and A. Bohrdt, “Feshbach resonance in a strongly repulsive bilayer model: a possible scenario for bilayer nickelate superconductors,” (2023),

- arXiv:2309.15843 [cond-mat.str-el].
- [55] “Supplementary material,” .
- [56] C. Hubig, F. Lachenmaier, N.-O. Linden, T. Reinhard, L. Stenzel, A. Swoboda, and M. Grundner, “The SYTEN toolkit,” .
- [57] C. Hubig, *Symmetry-Protected Tensor Networks*, Ph.D. thesis, LMU München (2017).
- [58] J. R. Schrieffer and P. A. Wolff, Phys. Rev. **149**, 491 (1966).
- [59] J. N. Fuchs, A. Recati, and W. Zwerger, Phys. Rev. Lett. **93**, 090408 (2004).
- [60] A. Recati, J. N. Fuchs, and W. Zwerger, Phys. Rev. A **71**, 033630 (2005).
- [61] I. V. Tokatly, Phys. Rev. Lett. **93**, 090405 (2004).
- [62] R. Citro and E. Orignac, Phys. Rev. Lett. **95**, 130402 (2005).
- [63] L. Homeier, In preparation. (2023).
- [64] H. Yang, H. Oh, and Y.-H. Zhang, “Strong pairing from doping-induced feshbach resonance and second fermi liquid through doping a bilayer spin-one mott insulator: application to  $\text{La}_3\text{Ni}_2\text{O}_7$ ,” (2023), arXiv:2309.15095 [cond-mat.str-el].

## SUPPLEMENTAL MATERIAL

### 1. Analysis of low and high doping limits - perturbative analysis

The black lines in Fig. 2 are the result of a perturbative expansion for  $t_{\parallel} \ll J_{\perp}$  in the low and high doping regimes, as in Ref [29]. In these limits the critical  $V_c$  to go from finite binding energies to vanishing binding energies becomes

$$V_c = J_{\perp} - 2t_{\parallel} + 5 \frac{t_{\parallel}^2}{J_{\perp}} \quad (6)$$

for the low doping case and

$$V_c = J_{\perp} - 4t_{\parallel} + 4 \frac{t_{\parallel}^2}{J_{\perp}} \quad (7)$$

for high doping.

### 2. Breaking of the SU(2) isospin symmetry

The effective sc description (3) is SU(2) symmetric in spins and isospins. However, the SU(2) symmetry of the isospins will break down if higher orders in  $t_{\parallel}/\Delta E$  are considered. This can also be seen in the numerical results when considering the  $x$ ,  $y$  and  $z$  components of the amplitudes of  $\langle \hat{J}_i \cdot \hat{J}_{i+1} \rangle$  in Fig. 4 separately, see Fig. 6. Note that  $\langle \hat{J}_i^x \cdot \hat{J}_{i+1}^x \rangle = \langle \hat{J}_i^y \cdot \hat{J}_{i+1}^y \rangle$  due to total  $\hat{J}^z$  conservation.

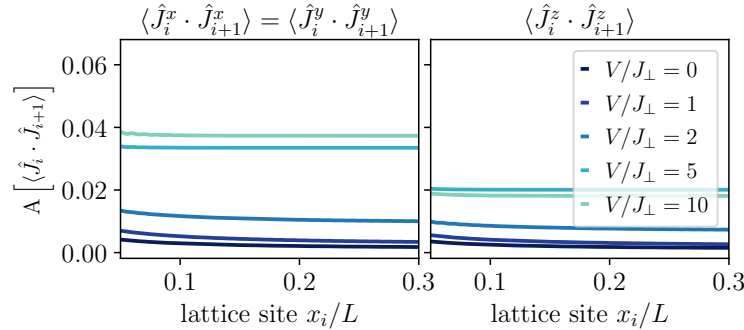


Figure 6. Amplitude of the VBS-like oscillations of  $\langle \hat{J}_i^a \cdot \hat{J}_{i+1}^a \rangle$  ( $a = x, y, z$ ) for the mixD ladder with  $t_{\parallel}/J_{\perp} = 1$ ,  $V/J_{\perp} = 5$ , length  $L_x = 200$  and  $\delta = 0.5$ .